HHS Public Access

Author manuscript

Mol Pharm. Author manuscript; available in PMC 2021 September 08.

Published in final edited form as:

Mol Pharm. 2020 September 08; 17(9): 3270–3280. doi:10.1021/acs.molpharmaceut.0c00390.

Inhalable nano-composite microparticles with enhanced dissolution and superior aerosol performance

Chune Zhu[a,b,*], **Jianting Chen**[b], **Shihui Yu**[b], **Chailu Que**[b], **Lynne. S. Taylor**[b], **Wen Tan**[c], **Chuanbin Wu**[d], **Qi Tony Zhou**[b,*]

[a]School of Traditional Chinese Medicine, Guangdong Pharmaceutical University, 280 Waihuan East Road, Guangzhou, 510006, China

[b]Department of Industrial and Physical Pharmacy, College of Pharmacy, Purdue University, 575 Stadium Mall Drive, West Lafayette, Indiana 47907, USA

[c]Institute for Biomedical and Pharmaceutical Sciences, Guangdong University of Technology, 100 Waihuan West Road, Guangzhou, 510006, China

[d]School of Pharmaceutical Sciences, Sun Yat-Sen University, 132 Waihuan East Road, Guangzhou, 510006, China

Abstract

Previous studies have shown that combining colistin (Col), a cationic polypeptide antibiotic, with ivacaftor (Iva), a cystic fibrosis (CF) drug, could achieve synergistic antibacterial effects against *Pseudomonas aeruginosa*. The purpose of this study was to develop dry powder inhaler (DPI) formulations for co-delivery of Col and Iva, aiming to treat CF and lung infection simultaneously. In order to improve solubility and dissolution for the water insoluble Iva, Iva was encapsulated into bovine serum albumin (BSA) nanoparticles (Iva-BSA-NPs). Inhalable composite microparticles of Iva-BSA-NPs were produced by spray-freeze-drying using water-soluble Col as the matrix material and L-leucine as an aerosol enhancer. The optimal formulation showed irregular-shaped morphology with fine particle fraction (FPF) values of 73.8 ± 5.2% for Col and 80.9 ± 4.1% for Iva. Correlations between "$D \times \sqrt{\rho_{tapped}}$" and FPF were established for both Iva and Col. The amorphous solubility of Iva is 66 times higher than the crystalline solubility in the buffer. Iva-BSA-NPs were amorphous and remained in the amorphous state after spray-freeze-drying as examined by powder X-ray diffraction. *In-vitro* dissolution profiles of the selected DPI formulation indicated that Col and Iva were almost completely released within 3 hours, which was substantially faster regarding Iva release than the jet milled physical mixture of the two drugs. In summary, this study developed a novel inhalable nano-composite microparticle using a synergistic water-soluble drug as the matrix material, which achieved reduced use of excipients for high-dose medications, improved dissolution rate for the water-insoluble drug and superior aerosol performance.

*Corresponding authors: Qi (Tony) Zhou, tonyzhou@purdue.edu; Chune Zhu, zhuchune1108@163.com.

Supporting Information

The Supporting Information is available free of charge.

The compositions of formulations are presented in Supporting Information to show the concentration of each component in each formulation.

Graphic Abstract

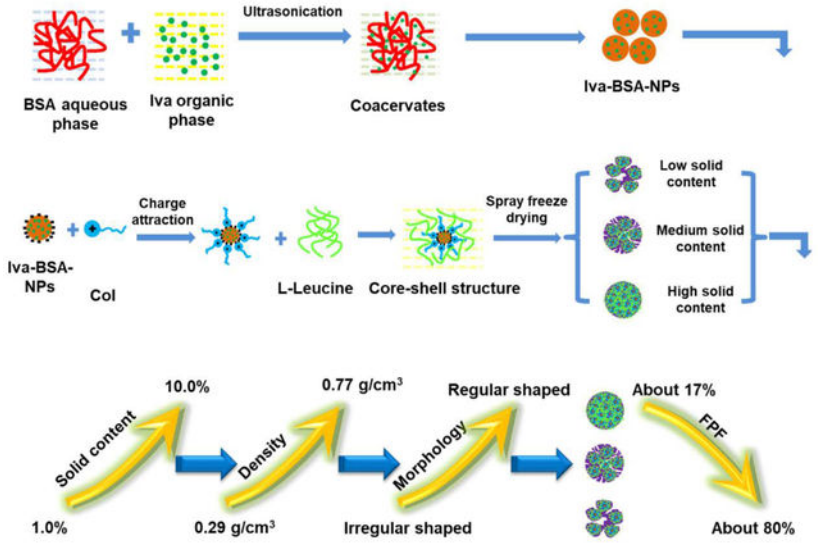

Keywords

Cystic fibrosis; Lung infection; Dry powder inhalers; Amorphous nanoparticle; Solubility; Dissolution

1. Introduction

Cystic fibrosis (CF) is an autosomal recessive disease triggered by mutations in the gene encoding the CF transmembrane conductance regulator (CFTR) protein[1]. Many organs such as lungs, pancreas, kidneys, and intestines are affected by CFTR mutations[2]. In the lung, mutations in the CFTR protein result in the production of thick and sticky mucus, which leads to airway obstruction, severe recurring infection, inflammation and eventual lung failure[3]. Recent studies have identified the main bacterial species underlying lung infections in CF patients as *Staphylococcus aureus* (SA) and/or *Pseudomonas aeruginosa* (PA). Lung infections caused by SA and PA play a key role in morbidity and mortality in CF patients, which is why treating lung infection is one of the therapeutic goals for CF[4].

Ivacaftor (Iva), approved by the Food and Drug Administration (FDA) recently for the treatment of CF, is a CFTR “potentiator”. It extends the opening time of the ion channel formed by the CFTR protein[5, 6]. Due to the quinoline ring structure, Iva demonstrated antimicrobial activity against SA with a MIC of 8–32 mg/L[7, 8]. In addition, recent research reported that Iva has significant antimicrobial activity against PA when combined with polymyxin B[9].

Colistin (Col), which belongs to the polymyxin family, is a polycationic cyclic peptide that has potent bactericidal activity against Gram-negative bacteria including PA, *Acinetobacter baumannii* and *Klebsiella pneumoniae*[10]. The antibacterial mechanism of Col is due to strong electrostatic interactions between the positively charged drug molecule and the

negatively charged bacterial membrane[11]. Recently, due to the development of rapid resistance against first-line antibiotics, Col has been increasingly used as a last-line antibiotic against multidrug-resistant Gram-negative bacteria in CF patients[10, 12]. However, previous studies showed that the efficacy of parenteral Col for lung infections in CF patients is low due to the suboptimal delivery of parenterally administered Col to the infection sites at the surface of lungs[13]. Simply increasing the dose of parental Col is not an option due to dose-limiting severe nephrotoxicity[14]. In the past decade, inhaled Col has become a complementary therapy for lung infections in CF patients[13].

Pulmonary drug delivery system (PDDS) can directly deliver drugs to the lung to increase the local drug concentration and limit systemic adverse effects[15–17]. Among PDDS technologies, dry powder inhalers (DPIs) exhibit advantageous portability and stability[1819]. Co-delivery DPIs containing both Iva and Col are a promising approach for the treatment of CF and its associated lung infections. However, the solubilities of Iva and Col vary widely; the former is hydrophobic and the latter is hydrophilic. Consequently, it is necessary to improve the aqueous solubility of Iva so as to enhance its dissolution and therapeutic activity in the lungs.

Nanoparticles have popular to improve drug physicochemical properties and formulation performance such as enhanced stability, controlled drug release and enhanced binding capacity of various drugs[20, 21]. Bovine serum albumin (BSA) is a widely employed nanocarrier attributed to its low cost, safety and non-immunogenicity[22, 23]. In addition, BSA is known to bind many compounds with different structures and solubility characteristics[24]. Moreover, the unique ligand-binding properties of BSA may improve the solubility and or dissolution of bound poorly water soluble drugs and enhance their bioactivity[25].

In this study, Iva-loaded BSA nanoparticles (Iva-BSA-NPs) were prepared by an antisolvent method to enhance Iva solubility. Then, DPI formulations for co-delivery of Col and BSA-Iva-NPs were produced by spray-freeze-drying. Literature has shown spray-freeze-drying may produce porous particles with low density and superior aerosol performance.[26, 27] The resultant formulations with different initial solid contents for the spray-freeze-drying feed solution were characterized regarding size distribution, true density, morphology, and *in-vitro* aerosolization properties. Also, *in-vitro* dissolution and cytotoxicity of the optimal formulation were determined.

2. Materials and methods

2.1. Materials

Ivacaftor (Iva) and colistin (Col) were purchased from AOKChem (Shanghai, China) and Betapharma Co. Ltd. (Jiangsu, China), respectively. Bovine serum albumin (BSA, purity > 98%, Mw 66.5 kDa), glutaraldehyde and L-leucine were supplied by Sigma-Aldrich Inc. (St. Louis, USA). 3-(4, 5-dimethylthiazol-2-yl)-2, 5-diphenyltetrazolium bromide (MTT) and acetonitrile (HPLC grade) were obtained from Thermo Fisher Scientific Inc. (Massachusetts, USA). The fetal bovine serum and Dulbecco's Modified Eagle Medium (DMEM) were purchased from Gibco Life Technologies Corporation (Eugene, USA). All other reagents and chemicals were analytical grade.

2.2. Determination of crystalline solubility and amorphous solubility for Iva

The equilibrium crystalline solubility in pH 6.8 buffer was determined by measuring the concentration of dissolved drug in a saturated solution. An excess amount of Iva was added to the buffer and the solution was stirred at 300 rpm for 48 h at 37 °C. The undissolved solid was removed from the saturated solution by ultracentrifugation (Optima L-100 XP, Beckman Coulter, Brea, CA) at 35000 rpm. The concentration in the supernatant was analyzed with a high performance liquid chromatography (HPLC) system (1260 Infinity, Agilent Technologies, Santa Clara, CA) with an Ascentis Express C18 column (10 cm × 3.0 mm, 2.7 μm, Sigma-Aldrich, St. Louis, MO). The mobile phase consisted of 60% acetonitrile and 40% water (v/v). A flow rate of 0.35 mL/min at 210 nm were used.

The amorphous solubility was measured by determining mass flow rate of Iva across a cellulose acetate membrane at different Iva concentrations.[28, 29] It has been shown that the flux across a membrane increases linearly with an increase in free drug concentration until the amorphous solubility is reached.[28] A side-by-side diffusion cell (PermeGear, Inc. Hellertown, PA) of 34 mL volume (donor or acceptor compartment) and 30 mm orifice diameter was used to evaluate Iva flux across the membrane at various Iva concentrations. A cellulose membrane with cutoff of 6–8 kDa was placed between the donor and acceptor compartments. Both the donor and acceptor compartments contained 33 mL of pH 6.8 phosphate buffer with 100 μg/mL hypromellose acetate succinate MF grade (HPMCAS-MF, to prevent crystallization of the drug in the buffer). Various aliquots of an Iva stock solution in dimethyl sulfoxide (5 mg/mL) were added to the donor compartment to achieve the desired concentration. Drug concentration in acceptor compartment was analyzed as a function of time by HPLC. At each sampling point, 100 μL of solution was withdrawn from the acceptor compartment. The slope of concentrations in the acceptor compartment *vs.* time when plotted represented the mass flow rate across the membrane. The mass flow rate across the membrane increased with an increase in concentration in the donor compartment, until the amorphous solubility was reached. At the concentrations above amorphous solubility, the maximum free drug concentration was reached, and the mass flow rate across the membrane remained unchanged. Thus, amorphous solubility of Iva was estimated as the concentration where the mass flow rate first reached the plateau value.

2.3. Preparation of Iva-BSA-NPs

Iva-BSA-NPs were produced by the antisolvent method with some modifications[20, 30, 31]. Initially, BSA and Iva with mass ratios of 20:2, 25:2 or 30:2 were dissolved in ultra-pure water and dimethyl sulfoxide (DMSO), respectively. The volume ratio of aqueous phase to organic phase was set at 3:1. The nanoparticles were obtained by a continuous dropwise addition of Iva solution into BSA solution at a constant rate of 1.0 mL/min under an ultrasonic dispersion (Ultrasonic Bath 5.7L, Thermo Fisher scientific Inc.). After the antisolvent process, glutaraldehyde solution (8.0%, v/v) was added into the nano-suspension at a volume ratio of 1:100 with magnetic stirring (400 rpm) for 24 hours at ambient temperature to fully crosslink the amino groups of BSA. Finally, the resulting Iva-BSA-NPs were obtained by centrifugation (16,000 g for 20 min), and were washed three times with ultra-pure water to eliminate free BSA, Iva and excess glutaraldehyde.

2.4. Preparation of DPI formulations by spray-freeze-drying for co-delivery Col and Iva-BSA-NPs

The co-delivery DPI formulations were prepared by spray-freeze-drying. L-leucine was used as the matrix and aerosol enhancer excipient in all formulations. The preparation process was slightly modified from the previous studies[32, 33]. Col solution (4.0 mg/mL) was mixed with an equal volume of Iva-BSA-NPs suspension (4.0 mg/mL). The doses here may not represent the final clinical doses, which should be optimized in *in-vivo* studies. The resultant suspensions were added to solutions of L-leucine to generate a total initial solid content of 1.0, 2.0, 3.0, 5.0, 8.0 or 10.0% w/w, which were termed as F1 to F6 respectively. It is worth pointing out that the maximum concentration of L-leucine was 20 mg/mL in this study. When the initial solid content can't achieve the preset value (1.0, 2.0, 3.0, 5.0, 8.0, 10.0%, respectively), Col was the supplemented matrix material in L-leucine solution. Therefore, in addition to being a drug, Col is also a matrix for dry powder particles in F3~ F6. Next, the suspension was pumped through an ultrasonic atomizer nozzle (9230 Flawil, Switzerland) into liquid nitrogen with the power set at 3.5 watt with a controlled feed rate of 2.0 mL/min. Subsequently, the atomized droplets were frozen, collected and transferred to a Labconco freeze dryer under vacuum (chamber pressure below 0.5 mbar) at −25°C for 48 hours to achieve the sublimation of solvents. Finally, the microparticles were collected and sealed in a desiccator with silica beads for further studies.

2.5. HPLC analysis

Iva and Col were analyzed by HPLC (1260, Agilent, Germany) for dispersion and dissolution studies as described previously with some modifications[34, 35]. An Eclipse plus C18 column (4.6×150 mm, 5 μm, Agilent, Santa Clara, USA) was employed for the simultaneous determination of Iva and Col. The mobile phase for Col was a mixture of 30 mM sodium sulfate solution (pH adjusted to 2.5 with H_3PO_4, 76% v/v) and acetonitrile (24% v/v), while for Iva was acetonitrile/water/methanol (3:1:0.17) mixture with pH 3.0 (pH adjusted with triethylamine). Flow rate was set as 1.0 mL/min and injection volume at 20 μL. Col was detected at 215 nm and Iva at 254 nm. Linearity was found at 0.5~100.0 μg/mL with correlation coefficients (R^2) of 0.995 for Col and 0.5~200.0 μg/mL with correlation coefficients (R^2) of 0.999 for Iva.

2.6. Characterization of Iva-BSA-NPs

2.6.1. Particle size and Zeta potential (ZP)—The prepared Iva-BSA-NPs were analyzed regarding particle size, polydispersity index (PDI) and ZP by Malvern Nano Series (ZS90, Malvern Instruments Ltd., Malvern, UK). Each parameter was measured in triplicate.

2.6.2. Encapsulation efficiency (EE%) of nanoparticles—During the preparation of Iva-BSA-NPs, the free Iva in the supernatant after centrifugation was collected and analyzed by HPLC. Then the EE% was calculated using the following equation.

$$EE\% = \left(1 - \frac{M_{\text{free Iva}}}{M_{\text{total Iva}}}\right) \times 100\,\% \quad \text{(Eq. 1)}$$

The $M_{free\ Iva}$ and $M_{total\ Iva}$ represent the unbound and the original concentration of added drug, respectively.

2.6.3. Morphology of nanoparticles—In order to examine the morphology of the optimal nanoparticles, a freeze dryer (Free zone 4.5, Labconco, Kansas City, USA) was used to lyophilize nanoparticles after being washed and collected. Samples were fixed onto double-sided tape and gold-coated at 40 mA for 60 s using a sputter coater (208 HR, Cressington Scientific Instruments, Watford, UK). Images were captured by a field emission scanning electron microscope (NOVA nano SEM, FEI Company, USA) at an acceleration voltage of 10.0 kV.

2.6.4. Crystallinity of nanoparticles—The physical state of the drug (crystalline or amorphous) in the optimal Iva-BSA-NPs were characterized by the powder X-ray diffraction (PXRD), using a physical mixture (PM) of BSA and Iva as the control. PXRD measurements were made using a SmartLab™ diffractometer, (Rigaku Americas, Austin, USA) with a Cu-Kα radiation source, operating at 40 kV and 44 mA. The scanning 2θ range was set as 5 to 60° with a scanning rate of 5°/min[36].

2.7. Characterization of DPI formulations

2.7.1. Particle size, tapped density and true density—The particle size of batches F1 to F6 was measured by a Malvern MasterSizer 3000 (Malvern Instruments, Malvern, UK) using a dry dispersion unit with air pressure of 2.0 bar, a refractive index value of 1.65 and feed rate vibration of 50%. The S_{pan} values were calculated by Eq. 2 based on D_{90}, D_{10} and D_{50}, which represent the volume diameter of particles at 90%, 10% and 50% levels, respectively. Samples were analyzed in triplicate.

$$S_{pan} = \frac{D_{90} - D_{10}}{D_{50}} \quad \text{Eq. 2}$$

The powder bulk density was defined as powder density without consolidation and determined by carefully pouring the powder into a 100 mL measuring cylinder. Tapped density (ρ_{tapped}) was determined by measuring the mass and volume of the powder after 1000 taps to ensure the density reach a plateau.

The true density of the co-delivery microparticles was determined using a Micromeritic Pycnometer (AccuPyc 1340, Micromeritics, USA). Each measurement was repeated five times.

2.7.2. Crystallinity of DPI formulations—Crystalline states of DPI formulations and the PM of BSA, Iva, Col, raw L-leucine and spray-freeze-drying (SFD) L-leucine were characterized by PXRD using a similar method as described above for the nanoparticles.

2.7.3. Morphology of DPI formulations—Morphology of the co-delivery microparticles (F1 through F6) were also observed by SEM as described above for the nanoparticles.

2.7.4. *In-vitro* aerosolization—

In-vitro aerosol performance of powder formulations was assessed using a Multi-Stage Liquid Impinger (MSLI) (Copley Scientific Limited, Nottingham, UK). Each sample (approximately 10 ± 2 mg) was loaded into #3 hydroxypropyl methylcellulose capsules (Qualicaps, Whitsett, USA). Five capsules were dispersed through a low-resistant RS01 DPI device (Plastiape S.p.A., Osnago, Italy) using a standard dispersion procedure of 2.4 s at 100 L/min to generate an approximately 4 kPa pressure drop across the inhaler[36]. The cutoff diameters for Stages 1 to 4 of the MSLI were 10.4, 4.9, 2.4, and 1.2 μm, respectively[36]. Drugs retained in each part of dispersion equipment were washed and dissolved by the Iva mobile phase. Emitted dose (ED) and fine particle fraction (FPF) were calculated by Eq. 3 and Eq. 4 respectively. Each sample was evaluated in triplicate.

$$\mathrm{ED}\,\% = \frac{\text{USP induction port} + S_1 + S_2 + S_3 + S_4 + \text{Filter}}{\text{Capsule} + \text{Device} + \text{USP induction port} + S_1 + S_2 + S_3 + S_4 + \text{Filter}} \times 100\,\% \quad \text{Eq. 3}$$

$$\mathrm{FPF}\% = \frac{S_3 + S_4 + \text{Filter}}{\text{USP induction port} + S_1 + S_2 + S_3 + S_4 + \text{Filter}} \times 100\,\% \quad \text{Eq. 4}$$

2.7.5. Flowability test of DPI formulations by FT4 Powder Rheometer—

The standard dynamic test was performed to characterize the flowability of DPI formulations using a FT4 Powder Rheometer (Freeman Technology Ltd., Tewkesbury, UK). The vessel was filled with 25 mL of powder, then the blades were rotated into the sample while the rotational torque and axial force were measured[37]. Each sample was conditioned with a tip speed of 100 mm/s and seven replicates, followed by variable tip speeds of 100, 70, 40, and 10 mm/s[38]. The flow properties are quantitatively expressed by the total energy (TE), basic flow energy (BFE), and specific energy (SE), where TE is derived from measurements of all forces acting on the rheometer blade when displacing powder after completion of the test cycle, while BFE and SE represent the energy required to move down and move up the blades through the powder, respectively[39].

2.8. Dissolution tests

Dissolution experiments were performed at 37.0 ± 1.0°C using a Franz cell (V6B, PermeGear Inc., USA) with the preset stirring speed of 600 rpm. Samples were fired into the next generation impactor (NGI, Copley Scientific Ltd., UK) with the flow rate of 100 L/min for 2.4 s to collect the aerosolized particles in the S4 plate (the cut-off mean aerodynamic diameter is 1.31μm) with a membrane (Whatman, Buckinghamshire, UK). Twenty milliliter of phosphate buffered saline (PBS pH 7.4) with 0.5% SDS was used as the *in-vitro* dissolution medium. The membrane containing the aerosolized powder was placed on the top of the Franz cell and fixed by a holder and a clamp, being in contact with the dissolution media[40, 41]. At each time point of 5, 10, 20, 30, 60, 120, 180 and 360 min, an aliquot of 100 μL dissolution medium was withdrawn and an equal volume of fresh media was added to maintain a constant dissolution volume. After the last time point, the membrane was rinsed using the dissolution media in the cell reservoirs to determine the total recovered dose. The

contents of Col and Iva were determined by HPLC, and each test was performed in triplicate.

2.9. Cytotoxicity of DPI formulations

The cytotoxicity of selected formulations were evaluated by the MTT assay using a human lung carcinoma cell line (A549 cells, ATCC, Manassas, VA, USA), which was cultured by DMEM supplemented with 10% (v/v) fetal bovine serum, penicillin (100 U/mL) and streptomycin (100 μg/mL). The cells were seeded on 96-well plates at a density of 1×10^4 cells/well and incubated under 5% CO_2 and 37°C until adherent growth. Afterwards, the medium was replaced by 100 μL fresh medium containing 2.0, 4.0, 8.0 and 16.0 μg/ mL of Iva, and then incubated for an additional 24 h or 48 h. Cells treated with pure fresh medium were used as the blank control group. At the end of incubation, culture medium containing drugs was substituted by fresh DMEM and MTT solution (9:1, v/v). Following another 4 h of incubation, the medium was removed and DMSO was added to dissolve the formazan crystals. Finally, the optical density (OD) value of each well was measured at 490 nm using a microplate absorbance reader (BioTek Instruments, Inc., Winooski, USA). Cytotoxicity of the samples, indicated by the relative cell viability, was calculated by the Eq. 5 (n=6):

$$\text{Relative cell viability}\,(\%) = \frac{\text{OD}_{\text{sample cells}}}{\text{OD}_{\text{control cells}}} \times 100\,\% \qquad \text{Eq. 5}$$

2.10. Statistical analysis

Data were presented as mean ± standard deviation (SD). One-way analysis of variance (ANOVA) was employed for statistical analysis using SPSS 19.0 software (IBM Corporation, Armonk, USA). The significant difference was recorded if $p<0.05$.

3. Results and discussion

3.1. Crystalline and amorphous solubility

The crystalline solubility of Iva in pH 6.8 buffer was 80.1 ± 3.7 ng/mL. The amorphous solubility was determined by measuring the diffusion mass flow rate versus Iva concentration in the donor chamber, shown in Fig. 1. When donor chamber concentration was below ~5–6 μg/mL, Iva mass flow rate across the cellulose membrane increased linearly as a function of Iva concentration in the donor compartment. At donor chamber concentrations above 5–6 μg/mL, the diffusion mass flow rate reached a plateau, indicating maximum free drug concentration had been achieved in the donor compartment. Thus, Iva amorphous solubility was determined as around 5–6 μg/mL. Amorphous Iva is approximately 60–70 times more soluble than crystalline Iva.

3.2. Characterization of Iva-BSA-NPs

3.2.1. Particle size, ZP and EE%—The main characteristics of Iva-BSA-NPs are presented in Table 1. The mean particle size of Iva-BSA-NPs was below 250 nm in all cases, with a relatively narrow size distribution, characterized by PDI values below 0.3. ZP was negative due to the charged groups of BSA and the negative charge increased with an

increase in the mass ratio of BSA. ZP is important to reduce the tendency of aggregation in the nano-suspension, and therefore to maintain physical stability[42]. Moreover, the negative surface charge of nanoparticles may enhance interactions with the positively charged Col through electrostatic charge, in the preparation of composite microparticles.

The EE% of Iva-BSA-NPs was higher than 70% due to the high binding capacity of the two main binding sites (sites I and II) of BSA with small molecule drugs[30]. The BSA to Iva ratio of 25:2 was selected as the optimal formulation for subsequent studies considering size, PDI, EE% and actual drug loading.

3.2.2. Morphology and crystallinity of nanoparticles—Representative SEM image of Iva-BSA-NPs (BSA: Iva=25:2) are shown in Fig. 2A, demonstrating spherical particles with a size below 200 nm, and a relatively uniform particle size distribution. PXRD diffractograms of the raw Iva and the PM of BSA and Iva showed sharp crystalline peaks (Fig. 2B). In contrast, Iva-BSA-NPs did not show peaks, suggesting nanoparticles were likely amorphous.

The formation mechanism of Iva-BSA-NPs is shown schematically in Fig. 2C. In the antisolvent process, with the addition of organic solvent to the BSA aqueous solution, BSA undergoes phase separation due to its diminished solubility[43]. Subsequently, based on the binding of protein with small drug molecules via Van der Waals interactions and hydrogen bonds, coacervates were formed[20, 25, 31]. Subsequently, the coacervates were further hardened, attributed to condensation reactions between aldehyde groups of glutaraldehyde and amino moieties of lysine residues or guanidino moieties of arginine residues[44, 45]. More importantly, this process converted the crystal form of Iva to the amorphous glassy state, which is likely to enhance water solubility and the dissolution rate of the poorly water soluble Iva.

3.3. Characterization of DPI formulations

3.3.1. Particle size and true density—The particle sizes of powder formulations with different initial solid contents for the spray-freeze-drying feed solution are shown in Fig. 3. With the increase in initial solid contents, the mean particle diameter was found to be larger. All formulations exhibited a Gaussian distribution with the S_{pan} value less than 2.0, which indicated a satisfactory uniformity of particle size.

The true density increased from 0.29 ± 0.01 to 0.77 ± 0.02 g/cm^3 with an increase in initial solid content of the spray-freeze-drying feed solution (Table 2).

3.3.2. Crystallinity of DPI powders—The PXRD results for powder formulations (F1 through F6), raw drugs (Iva and Col), BSA, raw L-leucine, PM, and SFD L-leucine are shown in Fig. 4A. Because the sharp crystalline peaks of raw L-leucine masked the peaks of other materials, L-leucine and PM results were excluded in Fig. 4B. The peaks in F1 to F6 correspond to the peaks of SFD L-leucine (e.g. at around 6˚, 12˚, 19˚, 24˚, 31˚ and 33˚ 2θ), but the sharp peaks present in raw Iva are not observed, indicating that Iva was amorphous in the DPI formulations. These results were consistent with the PXRD data for nanoparticles. L-leucine, is present in samples F1–6 in crystalline form.

3.3.3. Morphology of DPI formulations—Fig. 5 shows SEM micrographs of DPI formulations (F1~F6) at two different magnifications. Iva-BSA-NPs were visible in the microparticles for F1 and F2.

The effect of initial solid contents in the spray-freeze-drying feed solution on the morphology of powder is apparent. As the initial solid content increased from 1.0% to 10.0%, the morphology of particles changed from irregular to spherical. This could be due to low solid content fails to form a continuous matrix or because at low initial solid contents, particles are very fragile and collapse during lyophilization under vacuum, which are consistent with previous reports[26, 27].

3.3.4. Flow property of DPI formulations by FT4 Powder Rheometer—The powder flow properties are important to not only the DPI manufacturing processes such as filling powder into a capsule or a blister, but also the emitted dose.[47] The flow properties are shown in Fig. 6. The high repeatability of the initial seven tests indicates a stable rheology, and the sensitivity to flow rate is determined by tests eight to eleven[48]. As shown in Fig. 6A, F1 to F5 had constant TE in the initial seven tests with the exception of F6, reflecting the weaker resistance to forced flow for this system when compared with other formulations. During tests eight to eleven, F5 and F6 exhibited an increase in TE, which meant it needed more energy to move the blade through the samples. This is because the dense and spherical microparticles (F5 and F6) are more resistant to flow during the measurements. Therefore, the porosity of irregular microparticles with lower bulk density (Table 3) means that they are relatively less resistant to flow[48, 49]. Similarly, BFE (Fig. 6B) and SE (Fig. 6C) values of F1 to F6 were also showed the same variation tendency as the TE. Usually, BFE and SE were affected by the gravitational forces and the inter-particulate forces, respectively. And a high BFE and SE indicated the microparticles were hard to be driven by airflow, that was, the formulations with poor aerosolization properties.

3.3.5. Aerosolization properties of DPI formulations—The ED values of all formulations were higher than 90% and there was no significant difference between the formulations (p>0.05) (Table 2). An increase in initial solid content led to lower FPF values for both Col and Iva, except for F1. It is interesting that particles of F1 and F2 collapsed during freeze drying under vacuum. However, the irregular shape of collapsed particles did not compromise the FPF. The microparticles with lower initial solid contents in the spray-freeze-drying feed solution have lower true density and tapped density (Table 3), which leads to significant smaller aerodynamic diameter (D_{ae}) (Table 3) and better aerosol performance[50–53].

The particle D_{ae} is determined by the equation below[54]:

$$D_{ae} = D \times \sqrt{\frac{\rho}{\rho_0}} \quad \text{Eq. 6}$$

Where ρ is the mass density of the material, and ρ_0=1.0 g/cm^3. D is particle geometric diameter.

We have plotted the correlations between "$D \times \sqrt{\rho_{tapped}}$" and FPF in Fig. 7. ρ_{tapped} is used here as ρ.[54] It is clear that there is a strong correlation between these two parameters with R^2 values of 0.9341 for Col and 0.9091 for Iva.

F2 was selected for the dissolution study because it had the highest FPF value of 73.8 ± 5.2% for Col and 80.9 ± 4.1% for Iva.

3.4. Dissolution tests

F2 and the jet-milled PM counterpart were selected for dissolution tests. For the jet-milled PM, only 29.71 ± 7.86% of Iva dissolved within 180 min and less than 60% after 6 h (Fig. 8). This is attributed to the high hydrophobicity and low aqueous solubility of Iva molecules[55]. In contrast, about 94% of Iva was dissolved in 3 h for F2, and the dissolution rate was similar to the water-soluble Col. Such substantially enhanced dissolution is likely due to a combined effect of amorphous form, binding to BSA and nano-meter particle size of Iva in the Iva-BSA-NPs. Water-soluble materials such as Col also provide a fast-dissolving matrix to prevent the aggregation and facilitates the dispersion of nanoparticles in the dissolution medium.

3.5. Cytotoxicity of DPI formulations

The cytotoxicity study of F2 and the corresponding jet-milled PM was performed on A549 cell lines with concentrations ranging from 2.0 to 16.0 μg/mL. Fig. 9 shows the cell viability results. Compared with the blank control group, neither the DPI formulation nor the PM showed toxic effects on cells within 24 h in the concentrations studied. However, when co-incubated for 48 h, the cell proliferation of the group with a drug concentration of 16.0 μg/mL showed significant decreases for both DPIs and PM. This might be due to inhibitory effects of the drugs on the cells if the concentration exceeds the tolerance dose.

Previous studies have shown that a combination of polymyxin B and Iva with a concentration of 2 μg/mL and 8 μg/mL respective, displayed synergistic killing activity against polymyxin resistant PA isolates[9]. Statistical analysis revealed no significant difference ($p > 0.05$) in cytotoxicity between the control group and the DPI formulation or PM when the concentrations of both drugs are 8 μg/mL and below. However, caution should be taken for high concentration delivery of Iva more than 16 μg/mL to the human lungs due to potential toxicity.

4. Conclusions

Pulmonary delivery of the hydrophilic drug Col and the hydrophobic drug Iva by a dry powder inhaler directly to the lungs could be effective in treating cystic fibrosis and its complications such as multidrug resistant Gram-negative lung infections. In this study, Iva-BSA-NPs were generated by an antisolvent method to convert the crystalline form of Iva to amorphous nanoparticles with the goal of enhancing Iva dissolution. Novel inhalable nano-composite microparticle formulations were developed by dispersing Iva-BSA-NPs in a matrix composed of a water-soluble synergistic antimicrobial, Col, to achieve co-delivery.

It was demonstrated that the initial solid contents of feed solutions significantly affected the physico-chemical properties of DPI formulations, including morphology, particle size, true density, flow property and aerosolization. Correlations were established between "$D \times \sqrt{\rho_{tapped}}$" and FPF. The optimal composite DPI formulation had an irregular-shaped morphology and excellent aerosolization performance with an FPF value of 73.8 ± 5.2% for Col and 80.9 ± 4.1% for Iva. More importantly, the formulation achieved up to 94% dissolution for Iva within 3 h, whereby Iva had a comparable dissolution rate to the water-soluble Col in the *in-vitro* dissolution test. Such synchronized dissolution behavior of two synergistic drugs is attributed to the substantially increased solubility of amorphous Iva, binding of Iva by BSA, and the use of the water-soluble Col as nano-composite matrix, whereby this co-delivery system could potentially demonstrate superior bioactivity. Future studies of *in-vivo* efficacy are warranted in an established mouse lung infection model[55–57].

Supplementary Material

Refer to Web version on PubMed Central for supplementary material.

Acknowledgements

Research reported in this publication was supported by the National Institute of Allergy and Infectious Diseases of the National Institute of Health under Award Number R01AI132681. The content is solely the responsibility of the authors and does not necessarily represent the official views of the National Institute of Health. Chune Zhu was financially supported by the Natural Science Fund Project of Guangdong Province (Grant No. 2018A030310555) and the Seedling raising funds of School of Traditional Chinese Medicine, Guangdong Pharmaceutical University (Grant No. YM1907). Donations of the RS01 DPI device from Plastiape S.p.A. and the HPMC capsules from Qualicaps, Inc. are acknowledged.

Abbreviations:

BFE	basic flow energy
BSA	bovine serum albumin
CF	cystic fibrosis
CFTR	Cystic fibrosis transmembrane conductance regulator
Col	colistin
DMEM	Dulbecco's Modified Eagle Medium
DMSO	dimethyl sulfoxide
DPI	dry powder inhaler
ED	Emitted dose
EE	Encapsulation efficiency
FDA	Food and Drug Administration
FPF	fine particle fraction

HPLC	high performance liquid chromatography
Iva	ivacaftor
Iva	BSA-NPs: Iva-loaded BSA nanoparticles
MSLI	Multi-Stage Liquid Impinger
MTT	3-(4, 5-dimethylthiazol-2-yl)-2, 5-diphenyltetrazolium bromide
NPs	nanoparticles
OD	optical density
PA	Pseudomonas aeruginosa
PBS	phosphate buffered saline
PDDS	Pulmonary drug delivery system
PDI	polydispersity index
PM	physical mixture
PXRD	powder X-ray diffraction
SA	Staphylococcus aureus
SE	specific energy
TE	total energy
ZP	Zeta potential

References

1. Garbuzenko OB; Kbah N; Kuzmov A; Pogrebnyak N; Pozharov V; Minko T Inhalation treatment of cystic fibrosis with lumacaftor and ivacaftor co-delivered by nanostructured lipid carriers. J Control Release 2019, 296, 225–231. [PubMed: 30677435]
2. Porsio B; Craparo EF; Mauro N; Giammona G; Cavallaro G Mucus and Cell-Penetrating Nanoparticles Embedded in Nano-into-Micro Formulations for Pulmonary Delivery of Ivacaftor in Patients with Cystic Fibrosis. Acs Appl Mater Inter 2018, 10, (1), 165–181.
3. McColley SA; Konstan MW; Ramsey BW; Elborn JS; Boyle MP; Wainwright CE; Waltz D; Vera-Llonch M; Marigowda G; Jiang JG; Rubin JL Lumacaftor/Ivacaftor reduces pulmonary exacerbations in patients irrespective of initial changes in FEV1. J Cyst Fibros 2019, 18, (1), 94–101. [PubMed: 30146268]
4. Katherine Fesen PS, Fuentes Nathalie, Nicoleau Marvin, Rivera Lidys, Kitch Diane, Graff Gavin R., Siddaiah Roopa. The role of microRNAs in chronic pseudomonas lung infection in Cystic fibrosis. Respiratory Medicine 2019, 151, 133–138. [PubMed: 31047110]
5. Hamilton CM; Hung M; Chen G; Qureshi Z; Thompson JR; Sun BY; Bear CE; Young RN Synthesis and characterization of a photoaffinity labelling probe based on the structure of the cystic fibrosis drug ivacaftor. Tetrahedron 2018, 74, (38), 5528–5538.
6. Hubert D; Chiron R; Camara B; Grenet D; Prevotat A; Bassinet L; Dominique S; Rault G; Macey J; Honore I; Kanaan R; Leroy S; Dufeu ND; Burgel PR Real-life initiation of lumacaftor/ivacaftor combination in adults with cystic fibrosis homozygous for the Phe508del CFTR mutation and severe lung disease. J Cyst Fibros 2017, 16, (3), 388–391. [PubMed: 28325531]

7. Reznikov LR; Abou Alaiwa MH; Dohrn CL; Gansemer ND; Diekema DJ; Stoltz DA; Welsh MJ Antibacterial properties of the CFTR potentiator ivacaftor. J Cyst Fibros 2014, 13, (5), 515–519. [PubMed: 24618508]
8. Thakare R; Singh AK; Das S; Vasudevan N; Jachak GR; Reddy DS; Dasgupta A; Chopra S Repurposing Ivacaftor for treatment of Staphylococcus aureus infections. Int J Antimicrob Ag 2017, 50, (3), 389–392.
9. Schneider EK; Azad MAK; Han ML; Zhou Q; Wang JP; Huang JX; Cooper MA; Doi Y; Baker MA; Bergen PJ; Muller MT; Li J; Velkov T An "Unlikely" Pair: The Antimicrobial Synergy of Polymyxin B in Combination with the Cystic Fibrosis Transmembrane Conductance Regulator Drugs KALYDECO and ORKAMBI. Acs Infect Dis 2016, 2, (7), 478–488. [PubMed: 27626100]
10. Liu YH; Kuo SC; Yao BY; Fang ZS; Lee YT; Chang YC; Chen TL; Hu CMJ Colistin nanoparticle assembly by coacervate complexation with polyanionic peptides for treating drug-resistant gram-negative bacteria. Acta Biomater 2018, 82, 133–142. [PubMed: 30316023]
11. Moffatt JH; Harper M; Harrison P; Hale JDF; Vinogradov E; Seemann T; Henry R; Crane B; Michael FS; Cox AD; Adler B; Nation RL; Li J; Boyce JD Colistin Resistance in Acinetobacter baumannii Is Mediated by Complete Loss of Lipopolysaccharide Production. Antimicrob Agents Ch 2010, 54, (12), 4971–4977.
12. d'Angelo I; Casciaro B; Miro A; Quaglia F; Mangoni ML; Ungaro F Overcoming barriers in Pseudomonas aeruginosa lung infections: Engineered nanoparticles for local delivery of a cationic antimicrobial peptide. Colloid Surface B 2015, 135, 717–725.
13. Velkov T; Abdul Rahim N; Zhou Q; Chan H-K; Li J Inhaled anti-infective chemotherapy for respiratory tract infections: Successes, challenges and the road ahead. Advanced Drug Delivery Reviews 2015, 85, 65–82. [PubMed: 25446140]
14. Garonzik SM; Li J; Thamlikitkul V; Paterson DL; Shoham S; Jacob J; Silveira FP; Forrest A; Nation RL Population Pharmacokinetics of Colistin Methanesulfonate and Formed Colistin in Critically Ill Patients from a Multicenter Study Provide Dosing Suggestions for Various Categories of Patients. Antimicrob Agents Ch 2011, 55, (7), 3284–3294.
15. de Boer AH; Chan HK; Price R A critical view on lactose-based drug formulation and device studies for dry powder inhalation: Which are relevant and what interactions to expect? Advanced Drug Delivery Reviews 2012, 64, (3), 257–274. [PubMed: 21565232]
16. Smyth HD; Hickey AJ Carriers in drug powder delivery. American Journal of Drug Delivery 2005, 3, (2), 117–132.
17. Grasmeijer F; Lexmond AJ; van den Noort M; Hagedoorn P; Hickey AJ; Frijlink HW; de Boer AH New mechanisms to explain the effects of added lactose fines on the dispersion performance of adhesive mixtures for inhalation. PloS one 2014, 9, (1), e87825. [PubMed: 24489969]
18. Elsayed MMA; Shalash AO Modeling the performance of carrier-based dry powder inhalation formulations: Where are we, and how to get there? J Control Release 2018, 279, 251–261. [PubMed: 29574042]
19. Lin YW; Wong J; Qu L; Chan HK; Zhou QT Powder production and particle engineering for dry powder inhaler formulations. Current pharmaceutical design 2015, 21, (27), 3902–16. [PubMed: 26290193]
20. Fonseca DP; Khalil NM; Mainardes RM Bovine serum albumin-based nanoparticles containing resveratrol: Characterization and antioxidant activity. J Drug Deliv Sci Tec 2017, 39, 147–155.
21. Casa DM; Karam TK; Alves ADS; Zgoda AA; Khalil NM; Mainardes RM Bovine Serum Albumin Nanoparticles Containing Amphotericin B: Characterization, Cytotoxicity and In Vitro Antifungal Evaluation. J Nanosci Nanotechno 2015, 15, (12), 10183–10188.
22. Elzoghby AO; Samy WM; Elgindy NA Albumin-based nanoparticles as potential controlled release drug delivery systems. J Control Release 2012, 157, (2), 168–182. [PubMed: 21839127]
23. Casa DM; Scariot DB; Khalil NM; Nakamura CV; Mainardes RM Bovine serum albumin nanoparticles containing amphotericin B were effective in treating murine cutaneous leishmaniasis and reduced the drug toxicity. Exp Parasitol 2018, 192, 12–18. [PubMed: 30026113]
24. Fang R; Hao RF; Wu X; Li Q; Leng XJ; Jing H Bovine Serum Albumin Nanoparticle Promotes the Stability of Quercetin in Simulated Intestinal Fluid. J Agr Food Chem 2011, 59, (11), 6292–6298. [PubMed: 21542648]

25. Singh P; Kim YJ; Singh H; Ahn S; Castro-Aceituno V; Yang DC In situ preparation of water-soluble ginsenoside Rh2-entrapped bovine serum albumin nanoparticles: in vitro cytocompatibility studies. Int J Nanomed 2017, 12, 4073–4084.
26. Ogienko AG; Myz SA; Ogienko AA; Nefedov A; Stoporev AS; Melgunov MS; Yunoshev AS; Shakhtshneider TP; Boldyrev VV; Boldyreva EV Cryosynthesis of Co-Crystals of Poorly Water-Soluble Pharmaceutical Compounds and Their Solid Dispersions with Polymers. The "Meloxicam–Succinic Acid" System as a Case Study. Crystal Growth & Design 2018, 18, (12), 7401–7409.
27. Ogienko AG; Markov AV; Senkova AV; Logashenko EB; Salomatina OV; Myz SA; Ogienko AA; Nefedov A; Losev EA; Drebushchak TN Increasing bioavailability of very poorly water-soluble compounds. A case study of an anti-tumor drug, soloxolon methyl. J Drug Deliv Sci Tec 2019, 49, 35–42.
28. Mosquera-Giraldo LI; Taylor LS Glass–Liquid Phase Separation in Highly Supersaturated Aqueous Solutions of Telaprevir. Molecular Pharmaceutics 2015, 12, (2), 496–503. [PubMed: 25541813]
29. Raina SA; Zhang GGZ; Alonzo DE; Wu J; Zhu D; Catron ND; Gao Y; Taylor LS Enhancements and Limits in Drug Membrane Transport using Supersaturated Solutions of Poorly Water Soluble Drugs. Journal of Pharmaceutical Sciences 2014, 103, (9), 2736–2748. [PubMed: 24382592]
30. Kayani Z; Firuzi O; Bordbar AK Doughnut-shaped bovine serum albumin nanoparticles loaded with doxorubicin for overcoming multidrug-resistant in cancer cells. Int J Biol Macromol 2018, 107, 1835–1843. [PubMed: 29030194]
31. Bhushan B; Dubey P; Kumar SU; Sachdev A; Matai I; Gopinath P Bionanotherapeutics: niclosamide encapsulated albumin nanoparticles as a novel drug delivery system for cancer therapy. Rsc Adv 2015, 5, (16), 12078–12086.
32. Ali ME; Lamprecht A Spray freeze drying for dry powder inhalation of nanoparticles. Eur J Pharm Biopharm 2014, 87, (3), 510–517. [PubMed: 24657824]
33. Liao QY; Yip L; Cho MYT; Chow SF; Chan HK; Kwok PCL; Lam JKW Porous and highly dispersible voriconazole dry powders produced by spray freeze drying for pulmonary delivery with efficient lung deposition. Int J Pharmaceut 2019, 560, 144–154.
34. Wang SN; Yu SH; Lin YW; Zou PZ; Chai GH; Yu H; Wickremasinghe H; Shetty N; Ling JH; Li J; Zhou Q Co-Delivery of Ciprofloxacin and Colistin in Liposomal Formulations with Enhanced In Vitro Antimicrobial Activities against Multidrug Resistant Pseudomonas aeruginosa. Pharm Res-Dordr 2018, 35, (10).
35. Akram NM; Umamahesh M A New Validated RP-HPLC Method for the Determination of Lumacaftor and Ivacaftor in its Bulk and Pharmaceutical Dosage Forms. Orient J Chem 2017, 33, (3), 1492–1501.
36. Mangal S; Nie HC; Xu RK; Guo R; Cavallaro A; Zemlyanov D; Zhou Q Physico-Chemical Properties, Aerosolization and Dissolution of Co-Spray Dried Azithromycin Particles with L-Leucine for Inhalation. Pharm Res-Dordr 2018, 35, (2).
37. Zhao ZY; Huang ZW; Zhang XJ; Huang Y; Cui YT; Ma C; Wang GL; Freeman T; Lu XY; Pan X; Wu CB Low density, good flowability cyclodextrin-raffinose binary carrier for dry powder inhaler: anti-hygroscopicity and aerosolization performance enhancement. Expert Opin Drug Del 2018, 15, (5), 443–457.
38. Lu XY; Chen L; Wu CY; Chan HK; Freeman T The Effects of Relative Humidity on the Flowability and Dispersion Performance of Lactose Mixtures. Materials 2017, 10, (6).
39. Gnagne EH, P. J, Gaiani C, Scher J, Amani GN. Characterisation of flow properties of foutou and foufou flours, staple foods in west africa, using the FT4 powder rheometer. Food Measure 2017, 11, 1128–1136.
40. Wang WB; Zhou QT; Sun SP; Denman JA; Gengenbach TR; Barraud N; Rice SA; Li J; Yang MS; Chan HK Effects of Surface Composition on the Aerosolisation and Dissolution of Inhaled Antibiotic Combination Powders Consisting of Colistin and Rifampicin. Aaps J 2016, 18, (2), 372–384. [PubMed: 26603890]
41. May S; Jensen B; Wolkenhauer M; Schneider M; Lehr CM Dissolution Techniques for In Vitro Testing of Dry Powders for Inhalation. Pharm Res-Dordr 2012, 29, (8), 2157–2166.

42. Nosrati H; Sefidi N; Sharafi A; Danafar H; Manjili HK Bovine Serum Albumin (BSA) coated iron oxide magnetic nanoparticles as biocompatible carriers for curcumin-anticancer drug. Bioorg Chem 2018, 76, 501–509. [PubMed: 29310081]
43. Langer K; Balthasar S; Vogel V; Dinauer N; von Briesen H; Schubert D Optimization of the preparation process for human serum albumin (HSA) nanoparticles. Int J Pharmaceut 2003, 257, (1–2), 169–180.
44. Gawde KA; Sau S; Tatiparti K; Kashaw SK; Mehrmohammadi M; Azmi AS; Iyer AK Paclitaxel and di-fluorinated curcumin loaded in albumin nanoparticles for targeted synergistic combination therapy of ovarian and cervical cancers. Colloid Surface B 2018, 167, 8–19.
45. Merodio M; Arnedo A; Renedo MJ; Irache JM Ganciclovir-loaded albumin nanoparticles: characterization and in vitro release properties. Eur J Pharm Sci 2001, 12, (3), 251–259. [PubMed: 11113644]
46. Yu S; Wang S; Zou P; Chai G; Lin Y-W; Velkov T; Li J; Pan W; Zhou QT Inhalable liposomal powder formulations for co-delivery of synergistic ciprofloxacin and colistin against multi-drug resistant gram-negative lung infections. Int J Pharmaceut 2020, 575, 118915.
47. Zhou QT; Armstrong B; Larson I; Stewart PJ; Morton DA Understanding the influence of powder flowability, fluidization and de-agglomeration characteristics on the aerosolization of pharmaceutical model powders. Eur J Pharm Sci 2010, 40, (5), 412–421. [PubMed: 20433919]
48. Freeman R Measuring the flow properties of consolidated, conditioned and aerated powders - A comparative study using a powder rheometer and a rotational shear cell. Powder Technol 2007, 174, (1–2), 25–33.
49. Xuejuan Zhang ZZ, Cui Yingtong, Liu Fei, Huang Zhengwei, Huang Ying, Zhang Rui, Freeman Tim, Lu Xiangyun, Pan Xin, Tan Wen, Wu Chuanbin. Effect of powder properties on the aerosolization performance of nanoporous mannitol particles as dry powder inhalation carriers. Powder Technol 2018, 1–9.
50. Frijlink HW; De Boer AH Dry powder inhalers for pulmonary drug delivery. Expert Opin Drug Deliv 2004, 1, (1), 67–86. [PubMed: 16296721]
51. Rahimpour Y; Kouhsoltani M; Hamishehkar H Alternative carriers in dry powder inhaler formulations. Drug discovery today 2014, 19, (5), 618–26. [PubMed: 24269834]
52. D'Addio SM; Chan JGY; Kwok PCL; Prud'homme RK; Chan H-K Constant size, variable density aerosol particles by ultrasonic spray freeze drying. Int J Pharmaceut 2012, 427, (2), 185–191.
53. Ogienko AG; Bogdanova EG; Trofimov NA; Myz SA; Ogienko AA; Kolesov BA; Yunoshev AS; Zubikov NV; Manakov AY; Boldyrev VV; Boldyreva EV Large porous particles for respiratory drug delivery. Glycine-based formulations. Eur J Pharm Sci 2017, 110, 148–156. [PubMed: 28479348]
54. Vanbever R; Mintzes JD; Wang J; Nice J; Chen D; Batycky R; Langer R; Edwards DA Formulation and physical characterization of large porous particles for inhalation. Pharm Res-Dordr 1999, 16, (11), 1735–1742.
55. Lin L; Quan GL; Peng TT; Huang ZW; Singh V; Lu M; Wu CB Development of fine solid-crystal suspension with enhanced solubility, stability, and aerosolization performance for dry powder inhalation. Int J Pharmaceut 2017, 533, (1), 84–92.
56. Lin Y-W; Zhou Q; Onufrak NJ; Wirth V; Chen K; Wang J; Forrest A; Chan H-K; Li J Aerosolized Polymyxin B for Treatment of Respiratory Tract Infections: Determination of Pharmacokinetic-Pharmacodynamic Indices for Aerosolized Polymyxin B against Pseudomonas aeruginosa in a Mouse Lung Infection Model. Antimicrob Agents Ch 2017, 61, (8), e00211–17.
57. Lin Y-W; Zhou QT; Han M-L; Chen K; Onufrak NJ; Wang J; Turnidge JD; Howden BP; Forrest A; Chan H-K Elucidating the Pharmacokinetics/Pharmacodynamics of Aerosolized Colistin against Multidrug-Resistant Acinetobacter baumannii and Klebsiella pneumoniae in a Mouse Lung Infection Model. Antimicrob Agents Ch 2018, 62, (2), e01790–17.

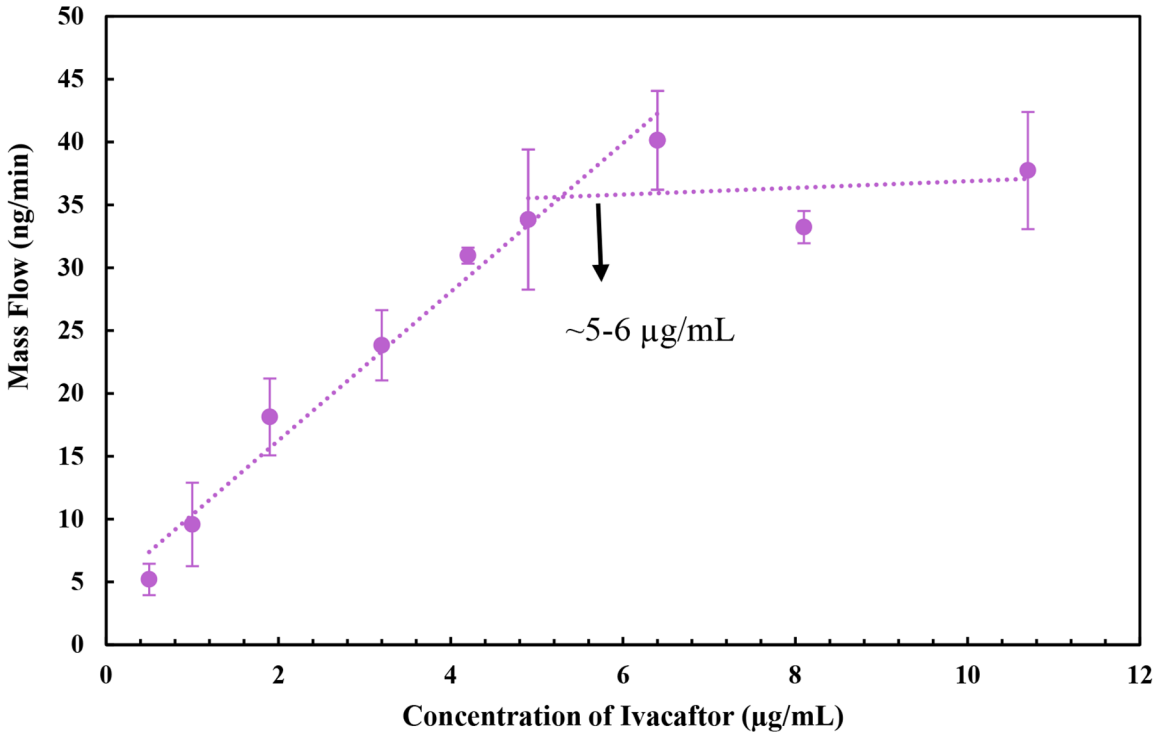

Fig. 1.

Diffusive mass flow rate versus Iva concentration in the donor compartment for determining amorphous solubility of Iva

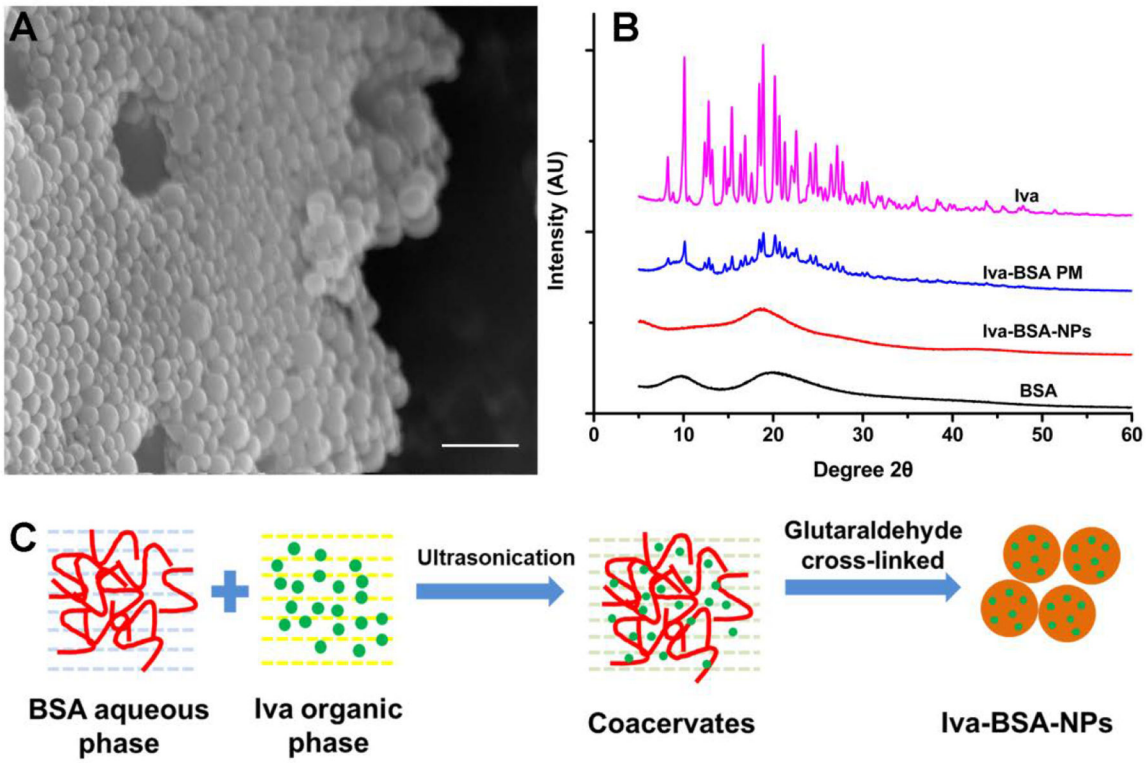

Fig. 2.

(A) SEM image of Iva-BSA-NPs with the scale bar of 500 nm; (B) PXRD patterns of Iva, PM of Iva and BSA, Iva-BSA-NPs and BSA; (C) schematic formation mechanism of Iva-BSA-NPs

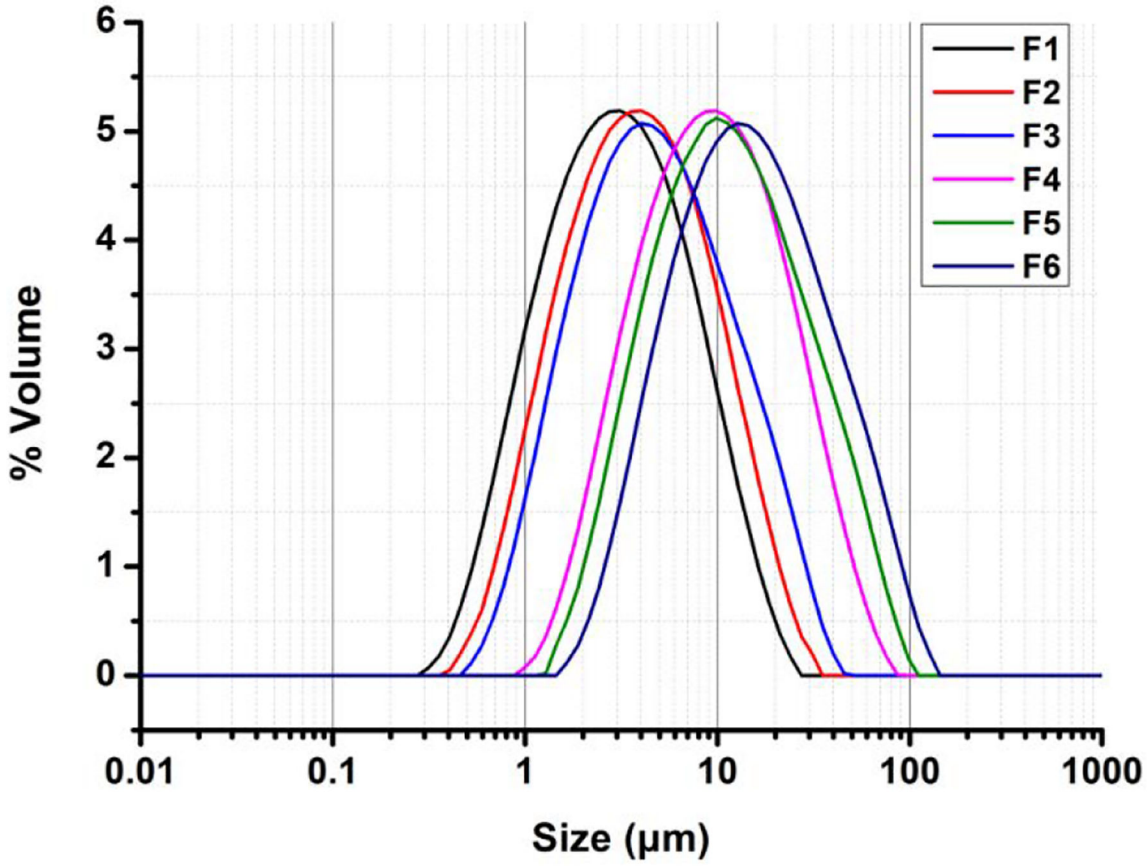

Fig. 3.
Particle size distributions of powder formulations with different initial solid contents in the spray-freeze-drying feed solution

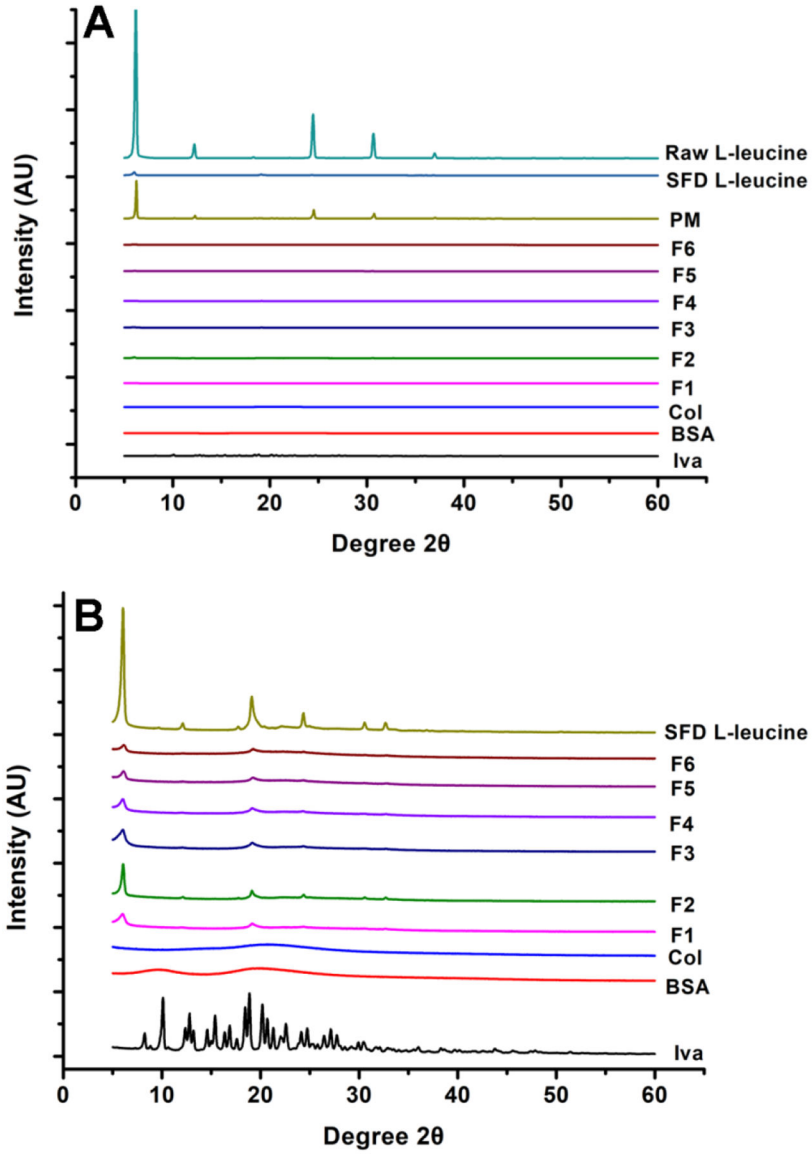

Fig. 4.

PXRD patterns of formulations, SFD L-leucine, raw materials and PM (A); PXRD patterns of above materials without displaying L-leucine and PM (B). SFD L-leucine data are reprinted from Yu et al.[46] with permission.

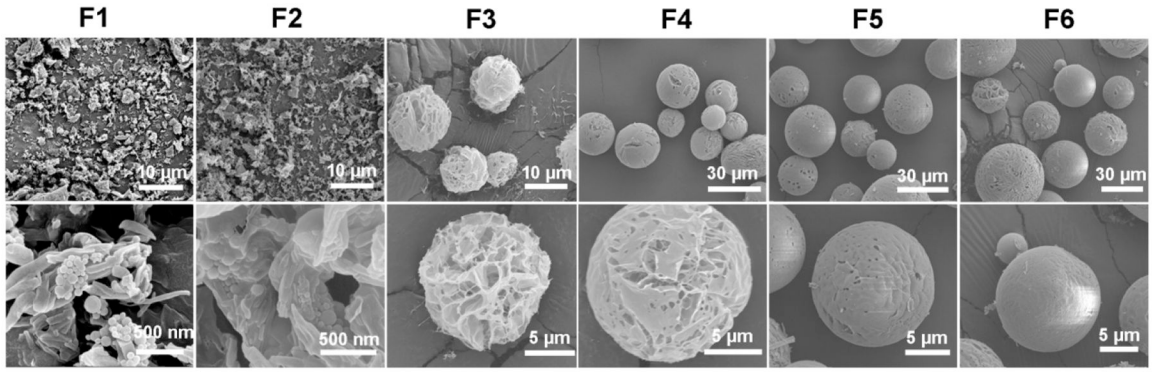

Fig. 5.
Representative SEM images for DPI formulations at two different magnifications

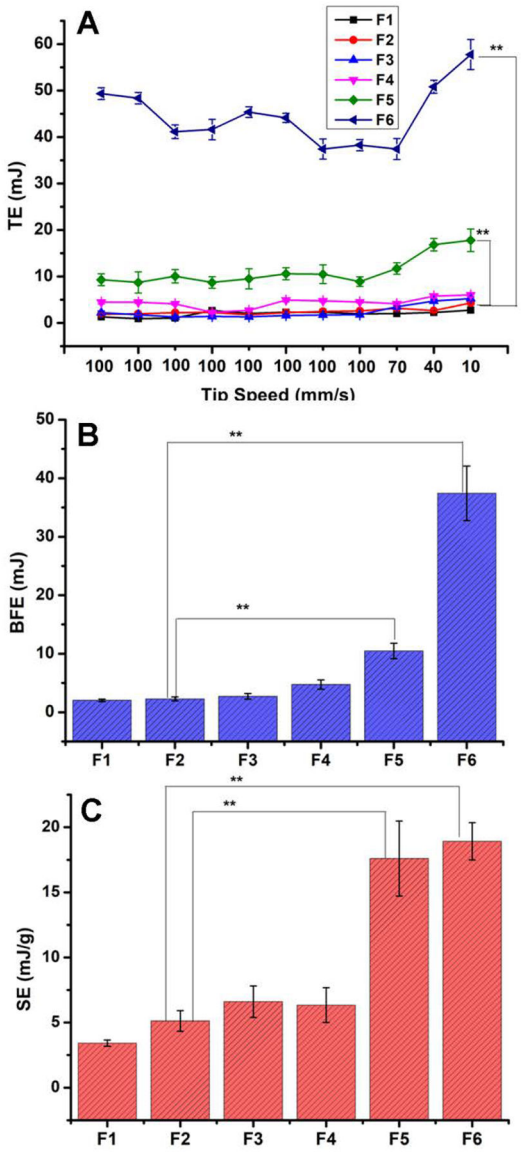

Fig. 6.

FT4 Dynamic test results (n=3). **represents p<0.01 as compared to F2

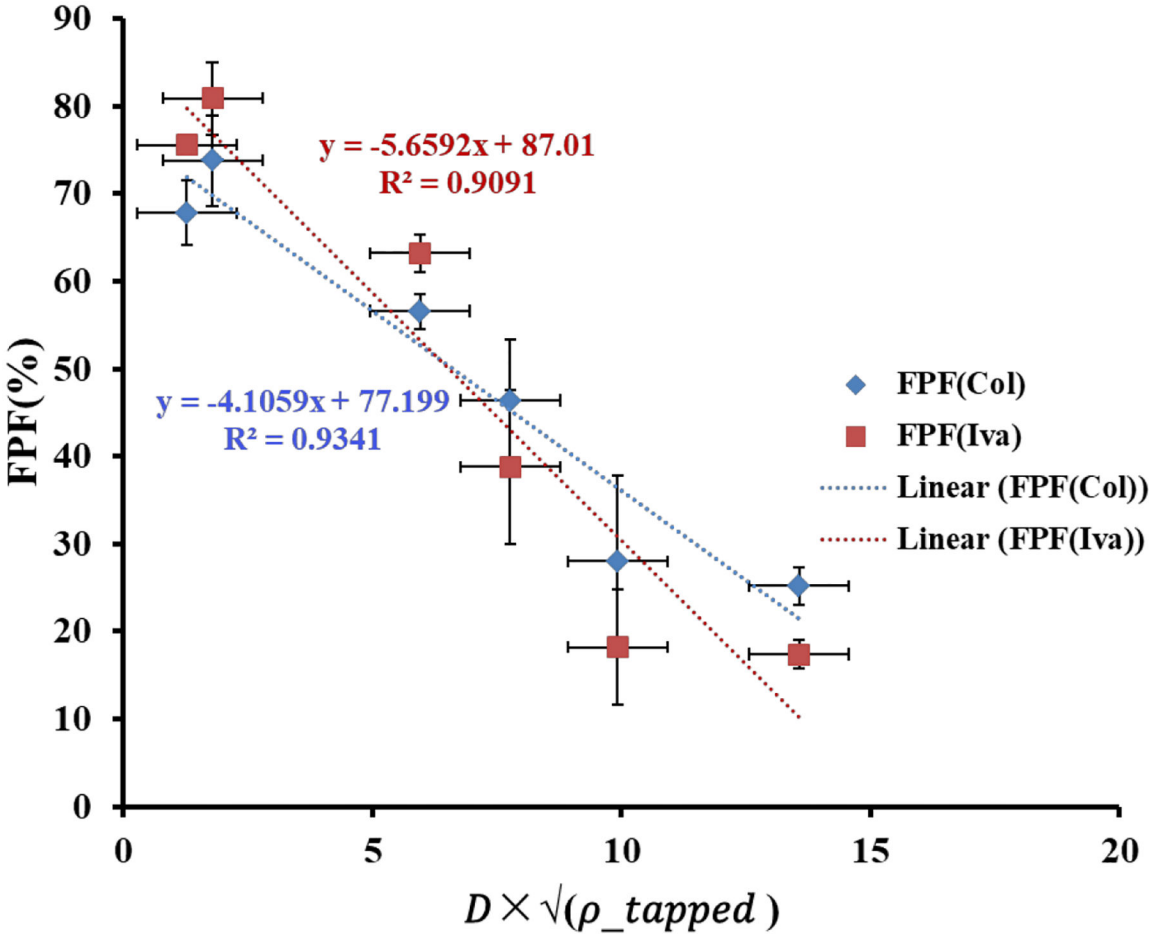

Fig. 7.

Correlations between "$D \times \sqrt{\rho_{tapped}}$" and FPF (mean ± SD, n=3)

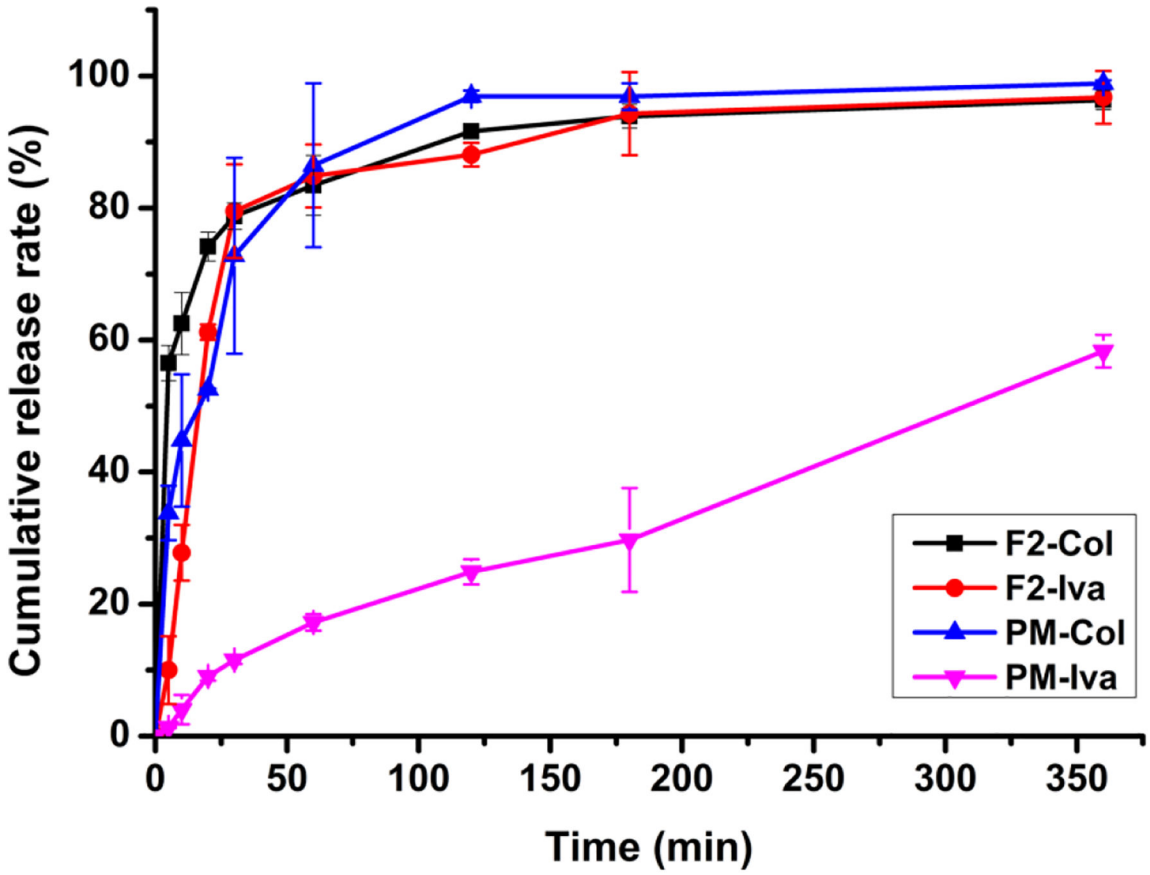

Fig. 8.
Dissolution profiles of F2 and the jet-milled PM counterpart ($n = 3$)

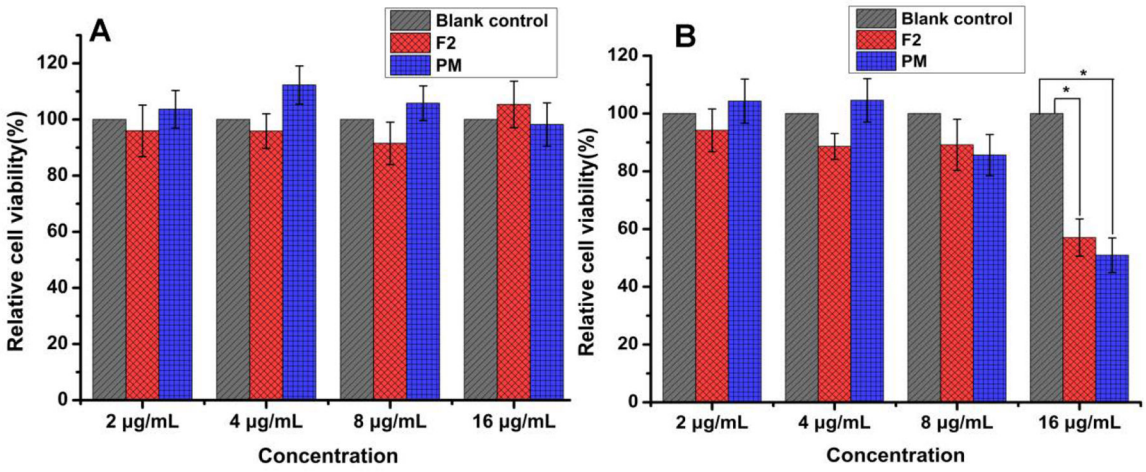

Fig. 9.

Cytotoxicity of DPIs (F2) and the corresponding jet-milled PM in A549 human cells (A: 24 h, B: 48 h, $n = 6$, mean ± SD). * means significant difference, $P < 0.05$

Table 1

Physico-chemical characteristics of Iva-BSA-NPs (n=3)

BSA: Iva (w/w)	Particle size (nm)	PDI	ZP (mV)	Actual drug loading%	EE%
20:2	234.5±6.5	0.22±0.09	−20.3±2.8	6.7±1.08	73.1±3.6
25:2	173.2±4.1	0.13±0.04	−27.9±3.0	5.8±0.31	78.7±2.6
30:2	171.5±4.3	0.14±0.03	−30.5±2.9	5.0±0.47	79.4±2.5

Table 2

Physico-chemical characteristics and *in-vitro* aerosolization properties of co-delivery DPI formulations with different initial solid contents in the spray-freeze-drying feed solution (mean ± SD)

F	Initial solid content (%)	True density (g/cm^3)[a]	ED (Col)[b]	FPF (Col)[b]	ED (Iva)[b]	FPF (Iva)[b]
F1	1.0	0.29±0.01	95.8±2.1	67.8±3.7	97.5±1.1	75.6±1.0
F2	2.0	0.31±0.01	97.4±1.5	73.8±5.2	96.4±2.0	80.9±4.1
F3	3.0	0.32±0.02	95.3±1.9	56.6±2.0	96.2±2.9	63.2±2.2
F4	5.0	0.43±0.01	96.5±3.4	46.4±6.9	96.4±3.2	38.8±8.8
F5	8.0	0.56±0.01	99.0±1.6	28.0±9.8	94.7±3.5	18.2±6.6
F6	10.0	0.77±0.02	94.9±2.3	25.2±2.1	91.9±1.3	17.4±1.6

[a] n=5;

[b] n=3

Table 3

Geometric diameter, aerodynamic diameter, bulk and tapped densities of co-delivery DPI formulations with different initial solid contents in the spray-freeze-drying feed solution (mean ± SD, n=3).

F	Geometric diameter (μm)	Bulk density (g/cm^3)	Tapped density (g/cm^3)	Aerodynamic diameter (μm)
F1	3.4±0.5	0.09±0.03	0.14±0.02	1.4±0.3
F2	4.1±0.4	0.12±0.02	0.19±0.02	2.0±0.2
F3	10.7±0.4	0.23±0.01	0.31±0.03	6.6±0.9 *
F4	12.6±0.6	0.30±0.02	0.38±0.02	8.5±1.4 *
F5	15.5±1.1	0.33±0.03	0.41±0.03	10.9±1.2 *
F6	17.1±1.5	0.51±0.04	0.63±0.02	14.9±2.7 *

* represents $p<0.05$ as compared to F2